Thick Film Solid-State Molecular Sensor for Acetylene Detection Based on n-n Heterojunction Semiconductor of Nanocrystalline Tungsten Oxide - Tin Oxide Compound

Yutthana Phimthong-Ngam*, Trakool Rummachat & Rangsan Jomtarak
Faculty of Science and Technology, Suan Dusit University

Abstract

Acetylene (C_2H_2) is widely used as a fuel and a raw material in many industry. Its combustion leads to explode with extreme violence in environment and safety control. A highly effective sensor for C_2H_2 detection is essential instrument for solving problem. Therefore, we aim to develop an effective thick film solid state molecular sensor based on n-n semiconductor heterojunction of nanocrystalline tungsten oxide-tin oxide (WO_3-SnO_2) compound in order to early detection of C_2H_2. We examine the effects of the nanostructure of sintered SnO_2 solid state gas sensors and the influences of W doped SnO_2 (WTO) concentration on the sensitivity and electrical properties to C_2H_2. The WTO gas sensor was fabricated by using the screen printing technique. The series of doped substrates with various WO_3 loadings from 1-70 wt.% were tested and measured for the electrical resistances in normal atmosphere and also for the sensor response to C_2H_2. The results showed that with W doping by range of 0.1-0.5 wt.%, the electrical resistances of films lowered significantly. Their optimal conditions for C_2H_2 sensor showed the sintering temperature (ST) of 600˚C for 6 h and the composition of 0.5 wt.% WTO at the optimum operating temperature of 300˚C. The C_2H_2 sensor sensitivities were further improved from 1.792 (pure SnO_2) to 2.527 through the best sensor prototype. The X-ray diffraction (XRD) study of an effective sensor revealed that SnO_2 contained a cassiterite phase and WO_3 contained a monoclinic phase, respectively. Scanning Electron Microscope (SEM) and Transmission Electron Microscope (TEM) investigations of the samples that sintered in air showed porous polycrystalline structures with spherical grain size ranging from 30-200 nm.

* Corresponding Author
e-mail: yutthana_phi@dusit.ac.th

Keywords : Solid-State Molecular Sensor, Acetylene, n-n Heterojunction Semiconductor, Tungsten Oxide-Tin Oxide (WO_3-SnO_2) Compound

Introduction

Acetylene gas (C_2H_2) is a colorless, flammable unsaturated hydrocarbon gas with a distinctive odor and the most effective one to identify thermal and electrical faults. It is widely used as a fuel in oxyacetylene welding and cutting of metals, as a raw material in various industrial and consumer products, such as paints, acetaldehyde, synthetic rubber, floor coverings, fabric, insecticide sprays and dry-cleaning solvents. Therefore, how to rapidly and accurately detect C_2H_2 gas is currently intensive research study nowadays. Generally, acetylene is not toxic, but when generated from calcium carbide, can contain toxic impurities such as traces of phosphine and arsine. Notable hazards are associated with its intrinsic instability, especially when it is liquefied pressurized, heated or mixed with air. Consequently, the combustion of acetylene can produce a large amount of heat, and it can explode with extreme violence if the absolute pressure of the gas exceeds 15 psi. Therefore, for environmental and safety purposes, the development of a highly effective C_2H_2 sensor has become increasingly important to meet the demands of accurate environmental monitoring which those objectives are for early leakage warning and for avoiding incomplete combustion. However, information on C_2H_2 sensors is still very limited in the literature (Jin, Chen, Zhou, Xiao & Yu, 2016). In this study, solid state molecular sensor (SSMS), metal-oxide semiconductor (MOS) gas sensor based on a change of the physical and/or chemical properties of sensing materials when exposed to various gas atmospheres, is introduced for being resistive type sensors. The detection principle of resistive sensors is based on changes in the resistance of a metal oxide thick film (semi-conducting in nature) upon adsorption of gas molecules that to be detected (Kanan, El-Kadri, Abu-Yousef & Kanan, 2009). The gas-solid interactions influence the density of electronic species in the film and thereby, the resistance of the film. Metal oxide sensors are also sometimes called chemiresistor. These are the simplest types of the gas sensors among the various technologies and hence perhaps are the most attractive gas sensor type for portable applications. They possess advantages of compact size, simple fabrication, low cost and simple measurement electronics. Chemiresistors tend to be broadly selective, responding to a large family of gases. The aim of this research is to

develop new sensors and sensor matrices that can improve the sensitivity and selectivity of sensors and decrease their power consumption (Wang, Yin, Zhang, Xiang & Gao, 2010). The tin (IV) oxide (SnO_2) has been the most extensively studied in gas sensing applications as a result of oxygen vacancies which are necessary for the gas-sensing mechanism, for example, it has a great response to target gasses at low working temperatures due to its non-stoichiometric. Furthermore, SnO_2 has a lower-cost when compares with other substances in the similar utilization area. The tungsten oxide (WO_3) is a chemical compound containing the transition metal tungsten and oxygen, whose electron density is ordinarily concluded by the stoichiometric defects concentration, for instance, vacancy of oxygen (Mohanta & Ahmaruzzaman, 2016). WO_3 is a promising sensing material as it presents great sensitivity to the detection of oxidizing gasses as a single-component oxide. It's electrical properties affect the WO_3 would be applied for several applications, for instance, photocatalyst, photochromic, electrochromic, etc. (Solis, Saukko, Kish, Granqvist & Lantto, 2001).

Objectives

1. To develop small thick film solid-state gas sensors with low power consumption and high sensitivity and selectivity for C_2H_2 detection

2. To verify the results of nanostructure and optimum composition to the C_2H_2 response of WTO

Research methodology: experimental design and validation

1. Fermi energy and schottky barrier control by the catalytic additives

Pure SnO_2, a band gap of 3600 meV, is an n-type semiconductor with the existence of the native donor levels that have energies of 30-34 meV and 140-150 meV under the conduction band edge and its inclusion of double and single ionizations of oxygen vacancies. The position of the Fermi level is positioned above the mid gap and it would be between the intrinsic Fermi level position and the conduction band edge because SnO_2 presents a negligible concentration of electronic band-gap states at their geometrically ideal surfaces (Haridas, Chowdhuri, Sreenivas & Gupta, 2008).

This situation, it started with an exact analytic solution to the equation of Poisson in one-dimensional under conditions of depletion.

$$\frac{\partial}{\partial x}\left(\varepsilon\frac{\partial\varphi(x)}{\partial x^2}\right)=-\rho(x) \quad (1)$$

where $\varphi(x)$ is the electric potential at distance x from the interface or surface plane, $\rho(x)$ is the charge density at the similar position and ε is the dielectric constant of the material.

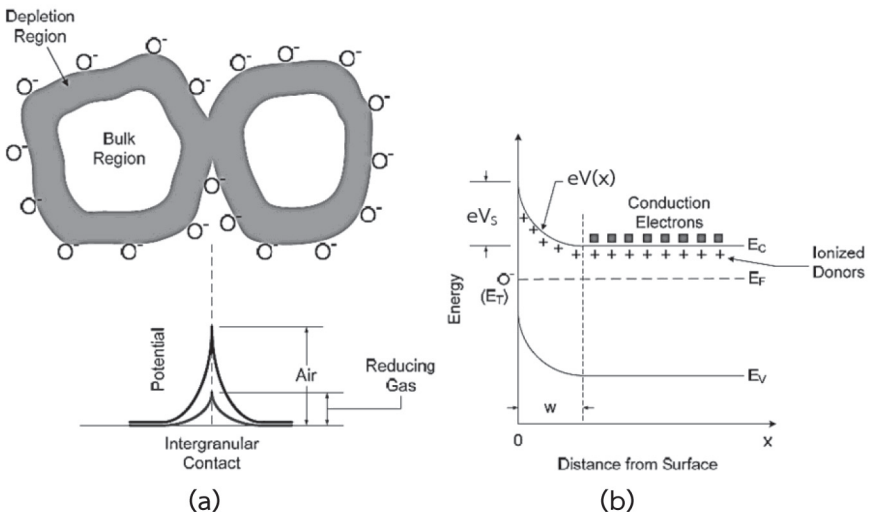

Fig. 1 Schematic model of (a) inter-grain Schottky barriers in the presence and absence of reducing gas and a band gap of SnO_2 (b) the relationship between energy and distance from surface

When considering that sufficiently large grain sizes have neutral regions inside, the contour conditions are:

$$\varphi\big|_{x=0}=V_s \text{ and } \frac{\partial\varphi}{\partial x}\bigg|_{x=W} \quad (2)$$

where V_S is the barrier height and W is the width of the space-charge region. Under rapid estimation, $\rho(x) = eN_D$ *is* the net charge density in the depletion region *(0<x<W)*, where N_D is the donor state density. By solving the Poisson's equation, the width of the depletion region is given by:

$$W = \sqrt{\frac{2\varepsilon V_s}{eN_D}} \tag{3}$$

and the charge per unit of area appearing in the depletion region will be given by:

$$Q_{SCR} = eN_D W = \sqrt{2\varepsilon e N_D V_S} \tag{4}$$

in view of only the surface states and applying the charge neutrality, the equation is:

$$\sqrt{2\varepsilon e N_D V_S} = Q_{SS} = e\int N_{SS}(E) f_{SS}(E, E_F) dE \tag{5}$$

this equation gives a barrier height of:

$$eV_S = \frac{Q_{ss}^2}{2\varepsilon N_D} = \frac{e^2}{2\varepsilon N_D}\left(\int N_{SS}(E) f_{SS}(E, E_F) dE\right)^2 \tag{6}$$

where N_{SS} is the net surface density, and f_{SS} is the occupancy probability by the Fermi-Dirac distribution. To compute the barrier height, it is necessary to introduce the particular model for the distribution of a state well below the Fermi level, which gives the recognized Schottky equation for planar geometry.

$$eV_S = \frac{e^2 N_{ss}^2}{2\varepsilon N_D} \tag{7}$$

Since surface states, $N_{ss}(E)$ and considering a density of states independent of the energetic position, $N_{ss}(E) = N_{ss}$, with $f_{ss}(E,EF)=0$ for $E>E_F$ and $f_{ss}(E,EF)=1$ for $E<E_F$, we have:

$$eV_S = \frac{e^2 N_{ss}^2}{2\varepsilon N_D}(E_F - E_V)^2 \tag{8}$$

Finally, to determine a density of states localized in E, $N_{ss}(E)=N_{ss}\delta(E-E_{ss})$,

$f_{ss}(\mathrm{E}) = \left[1 + exp(E - E_F / kT)\right]^{-1}$

$$eV_S = \frac{e^2 N_{ss}^2}{2\varepsilon N_D}\left[1 + exp\left(\frac{E_{ss} - E_F}{kT}\right)\right]^{-2} \quad (9)$$

where T and k are the absolute temperature and the Boltzmann constant (Samson & Fonstad, 1973).

In previous studies, the changes in the work function of the additive due to the presence of a gas caused a change in the Schottky barrier between the metal and the oxide and produced a change in conductivity. The adsorbed oxygen on the surface causes the extraction of electrons from the additive that dominates the depletion of charge carriers from the semiconductor surface. In order to modify or control the surface properties of the SnO_2, additives are usually included. The most important effects of additives are the increase of the maximum sensitivity and the rate of response as well as the reducing the temperature of maximum sensitivity.

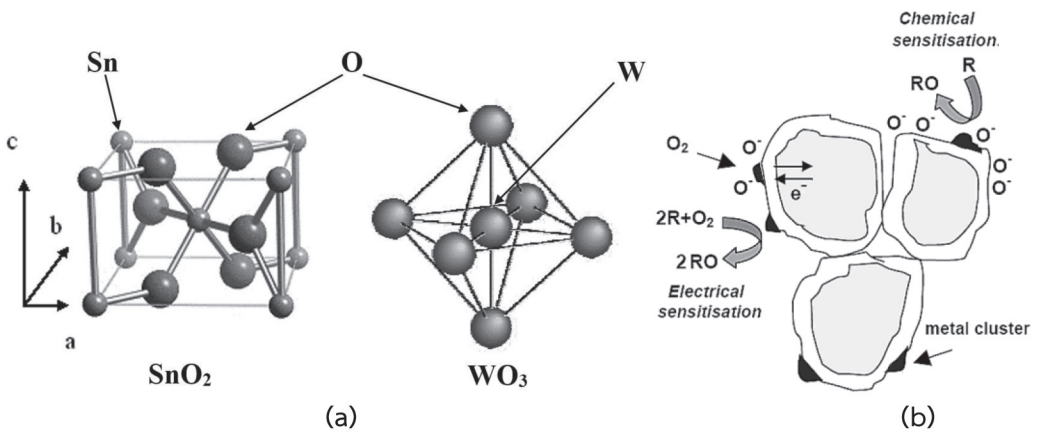

Fig. 2 (a) Model of crystalline SnO_2 and WO_3 structural (b) mechanism model of electrical and chemical sensitization of solid-state molecular sensor

A good dispersion of the additive particles such as the depleted regions at the surface of a metal-oxide overlap and the influence of the additive extends to the inter-granular contact. Moreover, the contact of the additive with the semiconducting oxide creates a barrier that is fully characterized by the electron affinity of the semiconductor, the work function of the metal and the density of surface states of the semiconductor that are located inside the energy band gap. All of these three contributions create a Schottky barrier through the formation of a depletion region in the semiconductor surface in contact with the cluster. Eventually, the surface states created by the presence of the additive can pin the Fermi level of the semiconductor to that of the additive (Yang et al., 2016)

2. WTO thick film sensor fabrication

In this work, an SnO_2 based type was used in this study; WO_3 was selected as a dopant to improve the response to C_2H_2 of the WTO sensor. Its precursor powder was prepared by *a sol–gel method* obtained by dispersing the nano powder in a suitable medium. Raw materials, listed in Table 1, were used as starting raw materials for the conventional oxide mixing process. The purity for each material was provided by the suppliers.

Table 1 Raw materials of sensor fabrication (Bai et al., 2010)

Materials	Purity (%)	Manufacturers
Tin(IV) Chloride ($SnCl_4 \cdot 5H_2O$)	Reagent grade	Sigma-Aldrich
Ammonium Tungstate Parapentahydrate ($(NH_4)_{10} \cdot W_{12}O_{41} \cdot 5H_2O$)	Reagent grade	Wako
Polyvinyl Alcohol Hydrolyzed	≥99.00	Sigma-Aldrich
Diethylene Glycol Monobutyl Ether	≥99.00	Sigma-Aldrich
Terpineol Anhydrous	Reagent grade	Fluka Chemicals
Ethyl Cellulose	Reagent grade	Fluka Chemicals
Ammonium Hydroxide (NH_4OH)	≥99.99%	Sigma-Aldrich
Nitric Acid (HNO_3)	≥90.0%	Sigma-Aldrich

The sol-gel method was performed by using distilled water to dissolve $SnCl_4 \cdot 5H_2O$ at a 0.05M concentration and it precipitated with NH_4OH in pH 8.0 solution. This solution was added drop-wise to deionize water at a temperature of 80 °C. The precipitated solution was aged for 4 h. Afterward, the Cl- anion was removed from the solution by centrifugation then washing with distilled water and dispersion in 0.1 M dilute acid solution. On account of the precipitation reaction, hydrated $SnCl_4 \cdot 5H_2O$ and hydrochloric acid were formed according to the equation (Teterycz & Licznerski, 2006).

$$SnCl_4 + xH_2O \xrightarrow{80^\circ C} SnO_2 \cdot (\mathrm{x}-2)\mathrm{H}_2O + 4HCl \qquad (10)$$

This homogenous precipitation technique was used to synthesize the WO_3 nano crystalline from aqueous $(NH_4)_{10}W_{12}O_{41} \cdot 5H_2O$ and HNO_3 solutions. The tungstate salt in deionized water and heated to 80°C. After vigorous stirring, a warm, concentrated nitric acid was added dropwise, so that the concentration for both reactants ranged from 5.0-16.0 mM. After continuous stirring, the mixed solution was kept at 80°C for 1 h; the precipitates were then allowed to settle for 20 h at 25 °C. The precipitate was washed by the addition of a large amount of deionized water and stirred for approximately 10 min. The precipitates were allowed to settle overnight before decanting the liquid. This washing procedure was performed twice. Finally, the precipitates were separated via ultrafiltration using a polymer membrane (pore size = 0.47 mm) after drying for 6 h at 110°C (Bai et al., 2010).

The additive techniques by the *impregnation method* basically consist of the evaporation of an aqueous solution of the metal. The solution is stirred together with powders of the semiconductor oxide and evaporated to dry, thereby precipitation of the metal salt by super-saturation of the solution. Therefore, without annealing, the oxidation state is that of the metal salt used as a precursor. WO_3 additive was added dropwise to the SnO_2 agitating solution for each experimental condition, the solution was stirred in a magnetic stirrer thoroughly, and the washing procedure was carried out six times. Finally, the precipitates were separated by filtration. The slurries were aged for 20 h then dried at 110˚C. Subsequently, the yield of powders were milled and sintered at temperatures from 500 to 1000˚C (heat rate=10˚C/min) for 4-6 h in air (Eom, Kim & Raju, 2013)

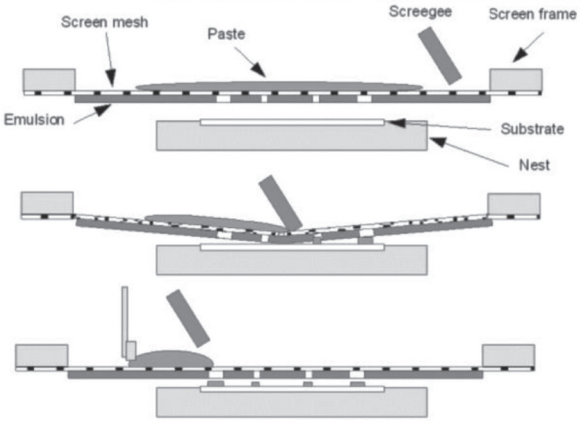

(a)

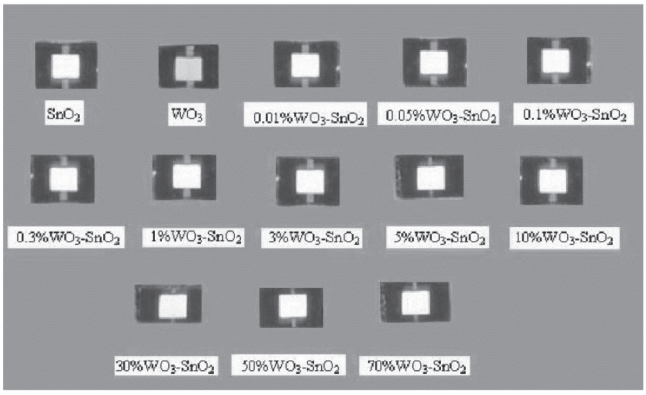

(b)

Fig. 3 (a) Schematic illustration of the sensor fabrication process (b) A sample of WTO sensor prepared by screen-printing technique

Thick film technology (TFT) is emerging as an important technique for a small-scale representation of electronic systems. Some of its main features include more flexibility and lower cost of design and production, higher frequency, power capability and good performance. Thus, in hybrid microelectronics this technique is more widely used than the thin film technique. Recently, TFT has been used in the production of chemical and a biological sensors. TFT can be used to produce geometrically well-defined, highly reproducible structures. These properties of a WTO sensor are highly desirable for chemical and biological applications and for the production of micron sized sensors. This is an advantage because minute sample volume will be required (Prasek et al., 2006).

The screen-printing method is a simple method used to prepare WTO sensor with good reproducibility, provided that the starting materials are well controlled, including the following major steps:

i. Preparation of the oxide pastes to be deposited.

ii. Printing of the prepared pastes onto suitable substrates.

iii. Drying of the prepared WTO at low temperatures (100-150˚C) to remove the light part of the organic vehicle.

iv. Firing at higher temperatures (>500˚C) to form a consolidated layer with the desired microstructure.

The pastes used for screen-printing were a mixture of nanometric powders and an organic vehicle combined with a small percentage of glass frit to improve the adhesion of the layers to the substrates. The thickness of the deposited layers was about 20–30 μm. The film underwent the following thermal treatments: the pure and doped samples were annealed at 650 and 850˚C. They were coated on the glass substrate with a painting brush to obtain a thick film of the sensor. The prepared thick film sensors were annealed at 600 ˚C overnight, prior to the sensing measurements. The actual temperature at the sample surface was within a 5% range of this set temperature. An average of 20-25 WTO of each type (pure and doped) was deposited. Among the deposited samples, five sensors of each type were selected for the gas sensing measurements (Khadayate, Waghulde, Wankhede, Sali & Patil, 2007).

3. Material characterization

Phase characterization can be accomplished by using X-ray diffraction analysis (XRD, JDX-3503), which it is an electromagnetic radiation with typical photon energies in the range of 100 eV-100 keV. X-rays primarily interact with electrons in atoms and during the course of the interaction, some photons from the incident beam are deflected away from the direction. For a given set of a lattice plane with an inter-plane distance of d, the condition for a diffraction (peak) to occur can be simply written as the Bragg's law (Yang & Zhao, 2008).

$$2d \sin\theta = n\lambda \tag{11}$$

where λ is the wavelength of the X-ray, θ the scattering angle, and n is an integer representing the order of the diffraction peak. The average size of crystallites was determined by the Debye-Scherrer formula (Smilgies, 2009), which is based on the analysis of the half width of peaks appearing on the diffractograms described by the equation:

$$D(2\theta) = \frac{K\lambda}{\beta \cdot \cos\theta} \tag{12}$$

where $D(2\theta)$ is the mean size of the crystalline domains, K is the shape factor of approximately 0.94 for particles of a spherical shape, λ is the X-ray wavelength, β is the full-width half maximum of the peak (FWHM) and θ is Bragg's angle (degrees).

A scanning electron microscope (SEM, JSM-6301F) was utilized to observe the morphology and particle size distribution of the WTO compound. For SEM specimen preparation, the WTO powder was attached to the holder with an adhesive tape, and then an evaporator for carbon film coating was used. The energy dispersive X-ray analysis (EDXA) was considered the chemical composition of the sensor powder. This technique employs X-rays that are emitted from the sample during the bombardment by the electron beam to characterize the elemental composition of the analyzed volume. The nanostructures of the compound have already been characterized via a high-Resolution Transmission Electron Microscopy (HRTEM, JEM-2010). The specimen of HRTEM is prepared by dissolving an amount of sensor powder on a particular solvent, deeply coating the carbon filmed grid in the solution, and removing the solvent via rotary evaporation. The specific surface area (SSA) and crystallite size (CS) of WTO powders were obtained by N_2

adsorption at -196.15 ˚C using a micrometrics gas adsorption analyzer (SA 3100) and calculated using the five-point Brunauer–Emmitt–Teller method (BET).

4. Gas response measurement

Characterization of the gas sensor response is an important feature to identify the various aspects of performance of the gas sensor in order to optimize its use. Because of the varied and complex mechanisms involved, the device operating conditions and the performance characteristics are highly interdependent. Testing at the development stage must also determine the parameters which need to be included in the essential performance tests for any sensors produced on a commercial basis. The response of a gas sensor is tested by measuring the resistance or conductance of the sensor element in air and in the presence of a known amount of the gas analyst (Šetkus et al., 2008). There are several measures of the performance of a gas sensor. They are often cited in the literature as sensitivity, selectivity and stability. Sensitivity (S), or sensor responses, consists of the change in the electrical resistance or conductance relative to the initial state upon exposure to oxidizing or reducing gas component which is defined as:

$$S = \begin{cases} \dfrac{R_{air}}{R_{gas}} \; for\ Reducing\ Gases \\ \dfrac{R_{gas}}{R_{air}} \; for\ Oxidizing\ Gases \end{cases} \qquad (13)$$

where R_{air} is the resistance in the synthetic air, and R_{gas} is the resistance in the oxidizing or reducing gases (Pimtong-Ngam, Jiemsirilers & Supothina, 2007). The sensitivity depends on many factors including the background gas composition, relative humidity level, sensor temperature, oxide microstructure, film thickness and gas exposure time. Also, selectivity is defined as the ability to discriminate a particular gas species from the back-ground atmosphere. Correspondingly, stability measures the capability of a sensor to maintain sensitivity for a particular gas species over durations of time (Smith, Vatelino, Falconer & Wittman, 1993).

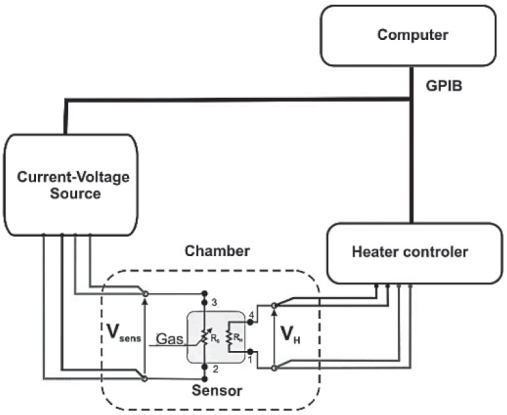

Fig. 4 Schematic diagram of the construction of gas sensor testing system (Suchorska-Woźniak, Rac, Fiedot & Teterycz, 2014)

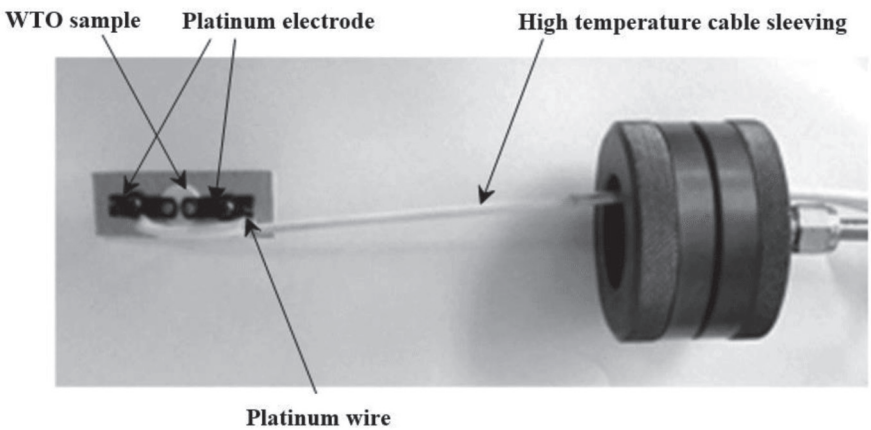

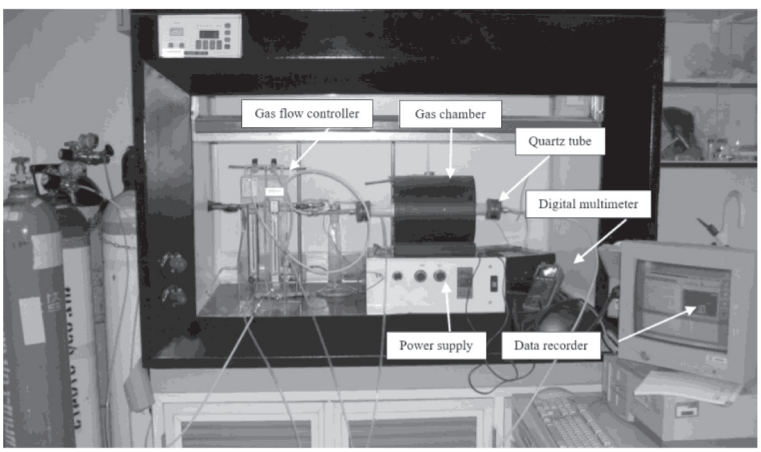

Fig. 5 Gas sensor testing system

The sensor compounds were pressed into a disc and applied to both sides of the platinum electrodes for a pre-test to C_2H_2. The sensitivity of the sensors was measured for C_2H_2 concentrations over a range from 1 to 20 ppm (controlled by two flow meters) at a temperature range of 250 to 450 ˚C. Prior to the start of the gas sensor testing system, the quartz tube was heated up to 450 ˚C for 2 h, in order to remove the adsorbates. Subsequently, we placed a sensor into a tube and flowed C_2H_2 over a test tube; the sensor's resistance was recorded by a digital multimeter, GPIB and data logger.

Results and Discussion

1. Phase and elemental chemical composition analysis

The XRD configuration of the WTO nano-compounds in 20 wt.% WTO and was used to evaluation the sizes of crystallite as presented in Fig 6.

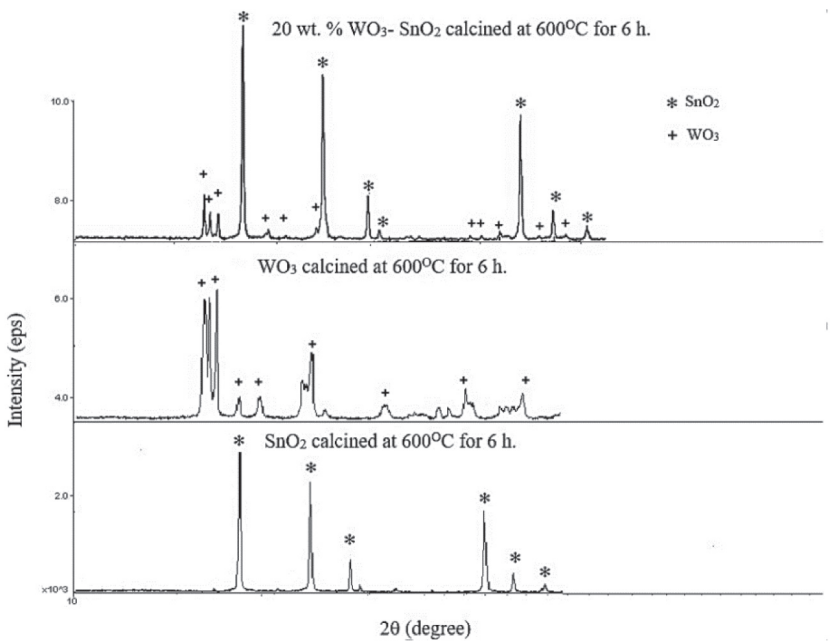

Fig. 6 XRD patterns of raw materials and 20 wt.% WTO sintered in air at 600 ° C for 6 hours.

The results of indexing the diffraction peaks of 0–20 wt.% WO_3, pure WO_3 and SnO_2 were found to be quite consistent with standard JCPDS data for WO_3 and SnO_2; no characteristic patterns of impurities were observed. The result suggests the association between the phase structure of raw materials and WTO. It is explaining the appropriate heating to a high temperature of 600 ˚C produces sufficient SnO_2 crystallinity without significant growth of crystallite, achieving the highest response.

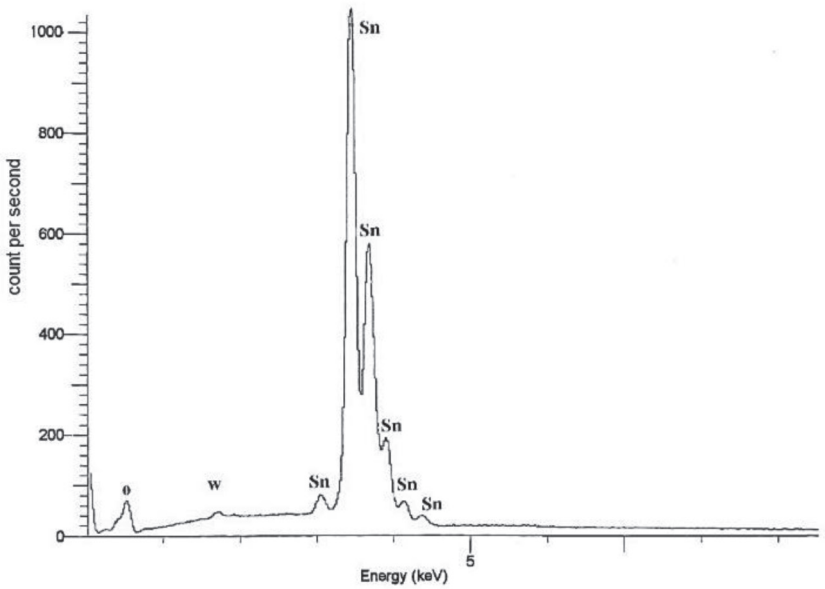

Fig. 7 EDXA spectrum of 0.1 wt.% WTO sintered in air at 600 ° C for 6 hours

From the EDXA spectrum of 0.1 wt.% WTO as shown in Fig. 7, the X-ray spectrum features visible are oxygen at energies of 0.5 keV and 1.70 keV, Sn at energies of 3.05, 3.45, 3.67, 4.15, and 4.37 keV. The quantitative analysis was run from the heights of peaks compared to the calibration standard elemental spectra.

2. Morphological characterization of WTO powder

The particle size and morphology of the 5% WTO nano-compounds sintered at 600°C were observed from HRTEM.

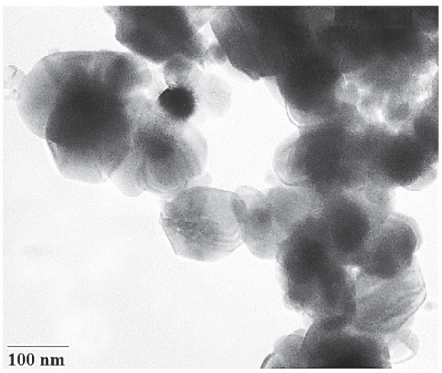

Fig. 8 HRTEM image of 5% WTO nano-compound sintered in air at 600°C for 6 h

The HRTEM image of the 5 wt.% WTO compound is shown in Fig. 8 showing the spherical shape and uniform size of the particles. The crystallite size was assessed by XRD, which is smaller than the average particle size observed from the HRTEM image. These results confirm the association between agglomeration of the crystallite and calcination process.

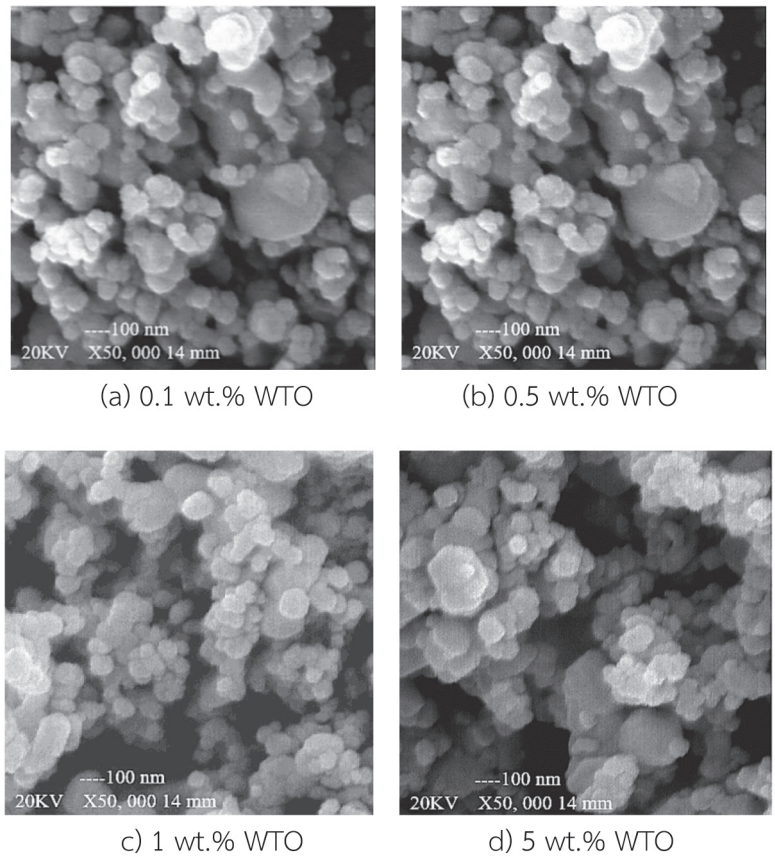

Fig. 9 SEM images of 0.1, 0.5, 1 and 5 wt.% WTO sintered at 600˚C for 6 h

Fig. 9 shows the SEM images of 0.1, 0.5, 1 and 5 wt.% WTO powder which consisted of spherical SnO_2 grains of various sizes, ranging from 30 to 200 nm. However, there were no obvious differences in the microstructure of the powder with W-doping. In order to give a reason for changes in sensor response, pore size distributions demonstrate that the pore volume of various pore sizes especially, a narrow pore size that it seemed to disturb the diffusion of a large gas molecule diffuse through the deep inside of sensing element. It was suggested that the decreased pore size was likely to be responsible for the decrease of sensor response to C_2H_2.

3. Effect of doping on crystallite size and specific surface area

The influences of complex admixtures on the specific surface area and crystallite size were considered using the BET that is shown in Fig. 10. It was based on the assumption that WTO powders consisted of interacted among each of the particles. The result suggested that particle aggregation and particle growth of the SnO_2 base were reduced by the WO_3 doping.

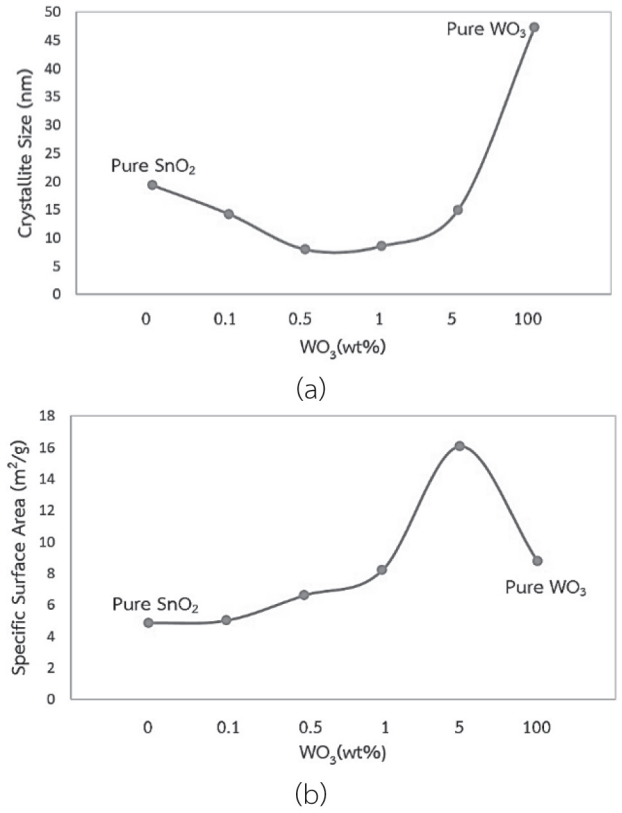

Fig. 10 (a) crystallite size and (b) specific surface area of the nano-compounds in various compositions

4. Effect of doping on gas response

As shown in Fig. 11 (a), the highest conductivities of the response curves were distinguishable and clearly seen in different that. Fig. 11 (b) that illustrated the conversions of sensor resistance of the 0.5 wt.% WTO sensors exposed to alternate streams of 4–10 ppm C_2H_2 gas and dry air. The results showed that the sensor had extremely rapid recovery time and response. The response was still a high response to dilute C_2H_2 below 10 ppm, which pointed out that the sensor created from the WTO nano-compound presenting high response to C_2H_2. The responses of the sensor were increased by the thermal energy had the highest value at optimum operating temperature. The previous study was shown a heterogeneous catalytic reaction that involved adsorption of reactants from the adsorbed gases onto a solid surface, surface reaction of adsorbed species, and desorption of products into the adsorbed gases. The chemical adsorption and rate of reaction slowly increased with heat transfer because of chemical adsorption and its required activation energy. While ratings of desorption were equivalent to that of adsorption and the optimal loading of chemisorbed oxygen ions was reached at the optimum operating temperature (≈ 300˚C), which would expedite the sensor to decrease C_2H_2 molecules, immediately giving the highest response. If the temperature was increased above 300˚C, the quantity of adsorbed gas would decline. Therefore, the sensor response decreased as a consequence of the declining gas response above the optimum operating temperature.

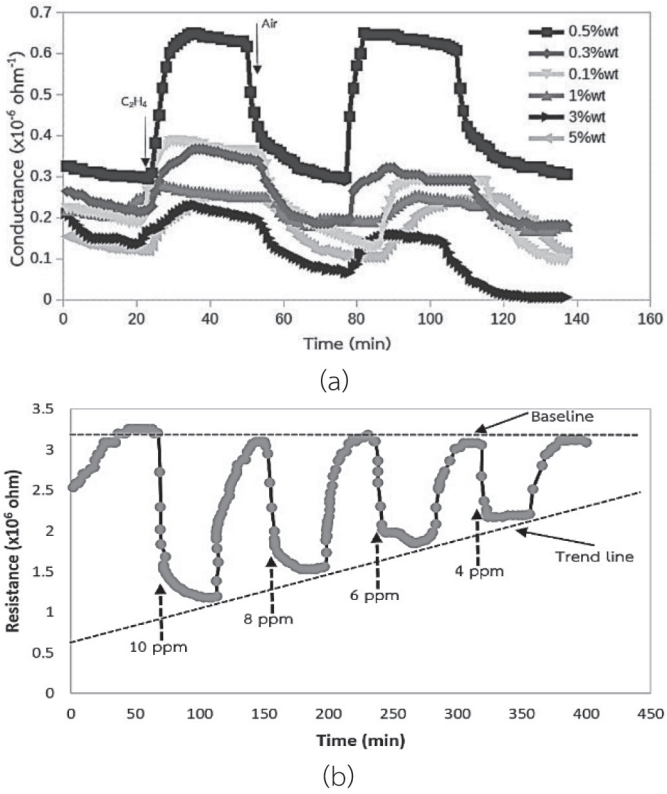

Fig. 11 A response curve of (a) nano-compounds sintered at 600˚C for 6 h in different compositions exposed to 8 ppm C_2H_2 gas and (b) the 5 wt.% WTO sensor at optimumoperating temperature of 300˚C exposed to 4–10 ppm C_2H_2 gas

WO_3 contents in compounds affected the gas response and that found at the 0.5% WTO nano-compound presented the highest response to 4-10 ppm C_2H_2 at the optimum operating temperature of 300˚C (Fig. 11 (b)). The response declined slowly with increased WO_3 content increased above 20%, as evidenced by decreased specific surface area (Fig. 10 (b)). Further analysis of the XRD pattern provides evident that when WO_3 content was below 40%, only SnO_2 diffraction peaks were founded. The higher WO_3 loaded compounds produced the XRD patterns of SnO_2 and WO_3 crystalline phase. The crystal formation of WO_3 was accompanied by reductions of specific surface area and sensitivity declined; this indicates that the WO_3 (<20 wt.%) may be available because the phases of amorphous covering on the SnO_2 crystallites acted as a barrier against the growing of grain boundaries of SnO_2 and efficiently inhibited the grain growth and the

decline in specific surface area during the sintering process (Yang, Lim & Han, 1999). In addition, lattice constants of the SnO_2 a and c obtained by the XRD data were 4.729 ˚A and 3.583A˚, respectively, which corresponded to the certainty of SnO_2. Furthermore, the substitutional decomposition of tungsten ions (W^{6+}) into the SnO_2 lattice is improbable, since the ionic radius of W^{6+} (0.60A˚) is dissimilar to that of tin ions (Sn^{4+}) (0.69A˚). Replacement of the W^{6+} ions in the lattice of SnO_2 leads to a discernible variation of parameters. The Schottky reactions for SnO_2 and WO_3, could written using Kröger-Vink notation:

$$WO_3 \underset{SnO_2}{\leftrightarrow} W_{Sn}^{\bullet\bullet} + 2O_O^X + O_i'' \quad (14)$$

$$WO_3 \underset{SnO_2}{\leftrightarrow} W_{Sn}^{\bullet\bullet} + 3O_O^X + \frac{1}{2}V_{Sn}'''' \quad (15)$$

$$SnO_2 \underset{WO_3}{\leftrightarrow} Sn_W^{//} + 2O_O^X + V_O^{\bullet\bullet} \quad (16)$$

The reduction of an oxide could written as the oxygen removal to the gas phase leaving behind oxygen vacancies:

$$O_O^X \leftrightarrow \frac{1}{2}O_2 + V_O^{\bullet\bullet} + 2e' \quad (17)$$

Previous exploration has shown the nano-compounds synthesis doped with WO_3 by impregnation of SnO_2 powders with solutions of ammonium tungstate. FTIR spectroscopy was observed for the nano-compounds comprising 1 mol.% and 5 mol.% WO_3. The results demonstrated that WO_3 increased the compounds transmittance, and this occurrence was associated with reductions of free electron quantities, leading toward the response improvement to target gas (Chiorino et al., 2001). This finding presented that the specific surface area of the WTO powders increased with increasing quantity of WO_3 loading to the SnO_2. Nevertheless, the results of the gas sensing test presented a different trend. That is, the WTO powder had a slight quantity of WO_3 and specific surface area had the greatest sensitivity, while the powder having the maximum specific surface area that exhibited the lowest sensitivity. This results further supported an idea of a mechanism of WTO in this system that did not depend on adsorption–desorption between the sensor surface and C_2H_2.

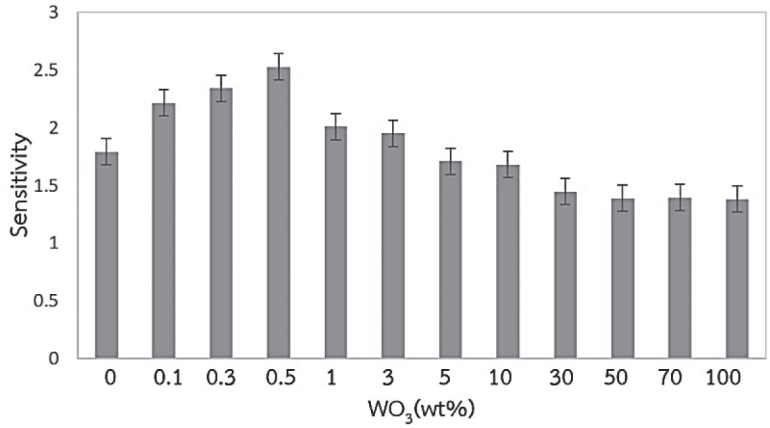

Fig. 12 Sensitivity of various WTO sensors towards 8 ppm C_2H_2 at optimum operating temperature of 300°C

The sensitivity of the WTO sensor of different admixtures was revealed in Fig. 12 it showed those sensitivities of various %WTO, pure WO_3 and pure SnO_2. Currently, previous study has reported that the sensitivity of the SnO_2 base was improved when a lesser quantity of the WO_3 (0.5 wt.%) was blended. Cumulative quantity of the WO_3 led to a reducing sensitivity.

5. Effect of optimum operating temperature

The sensitivities of the 0.5 wt.% WTO sensors to C_2H_2 were assessed at the operating temperature range from 200–500 °C. In Fig. 13, it demonstrated the sensitivity characterization pattern which derived from equation 13 at various operating temperature of the 0.5 wt.% WTO sensors towards 8 ppm C_2H_2. The optimum operating temperature at 300°C was the general value of the MOS gas sensor.

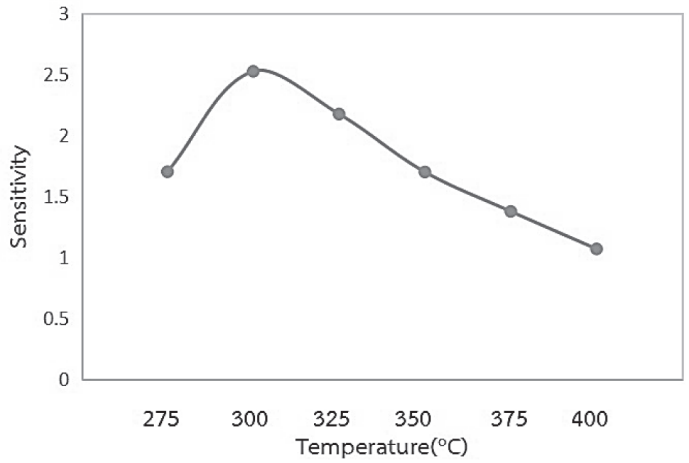

Fig. 13 Sensitivity pattern at various operating temperature of the 0.5 wt.% WTO sensors towards 8 ppm C_2H_2

6. Effect of sintering temperature

The WTO sensor was sintered at operating temperature to obtain enough crystallinity and structural stability for gas sensor detection. There were several possible explanation ways for this result: the thermal stabilities of the nano-compounds, the influences of the sintering temperature on H_2O_2 response and the 20% WTO nano-compound at various temperatures ranging from 500 -1000°C.

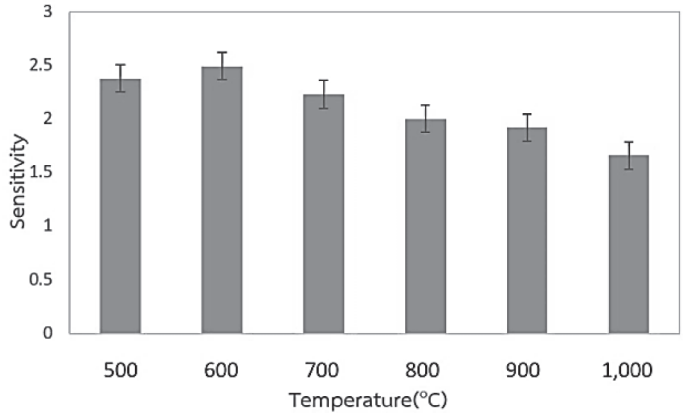

(a)

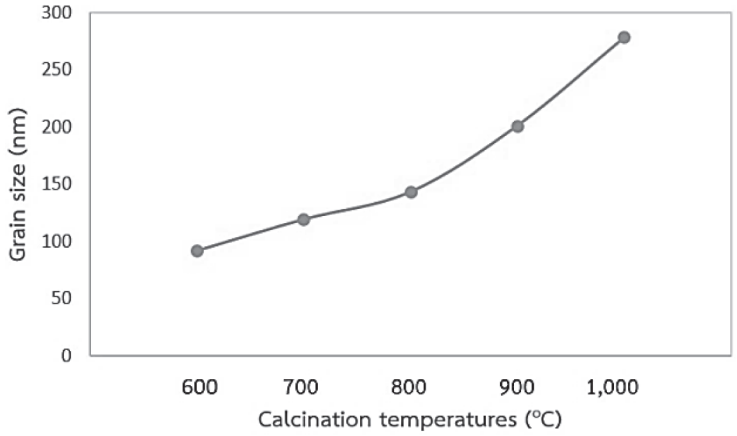

(b)

Fig. 14 (a) Sensitivity and (b) grain size of 0.5% WTO nano-compound sintered at various sintering temperatures to C_2H_2

In Fig. 14 (a), it illustrated the gradual reduction of sensitivity against increasing sintering temperature from 700-1000˚C. When sintering temperature was lower than 600˚C, for example, 400˚C, the compound had high specific surface area, but the response was low, demonstrating that the nano-compound's crystallinity did not co-operate with sensor stability. After each WTO samples was sintered at 600 ˚C, it explained the SnO_2 crystallites in the nano-compound had high stability. Even though sintering temperature Increased to 1000˚C, the response to C_2H_2 was significantly and drastically reduced because of enlarged compound crystallite size and decreased specific surface area. It was founded that the stabilities of nano-compound were higher than that of the single oxide. This may be a result of presence of grain interface between crystallite growth, nearby grains, and the cation interdiffusion, in spite of the surface energy stored at the boundaries. However, it is essential to know that as sintering temperature increases, the additive's optimizing effect becomes less evident.

Conclusion

WTO sensor compounds had WO_3 content in the range of 0.1–70.0 wt.% with uniform distribution of range from 30-200 nm. The sensor base was prepared by precipitation of hydrated WO_3 in the tungstate solution containing SnO_2 powder. The two

crystalline phases were stable up to at least 1000˚C. The WTO thick-films were sensitive to 0-10 ppm C_2H_2 gas at moderate optimum operating temperature. The sensitivity was largely depended on the amount of the WO_3. The 0.5 wt.% WTO sensor was the most sensitive, while the others were less sensitive compared to pure SnO_2. The incorporation of WO_3 suppressed SnO_2 grain growth and loss in surface area up to sintering temperature of 600˚C and markedly enhanced the thermal stability of SnO_2 and its response to C_2H_2, as confirmed by XRD, TEM, SEM and BET. The sensitivity to C_2H_2 was significantly affected by the composition of compound, the sintering temperature of the precursor and the optimum operating temperature of the sensor for certain gas concentrations.

Acknowledgements

This research was supported in part by Thailand's national budget for research (National Research Council of Thailand), in the 2008 fiscal year.

References

Bai, S., Li, D., Han, D., Luo, R., Chen, A., & Chung, C. L. (2010). Preparation, characterization of WO_3–SnO_2 nanocomposites and their sensing properties for NO_2. *Sensors and Actuators, B: Chemical,* 150(2), 749-755.

Chiorino, A., Ghiotti, G., Prinetto, F., Carotta, M. C., Malagù, C., & Martinelli, G. (2001). Preparation and characterization of SnO_2 and WO_x–SnO_2 nanosized powders and thick films for gas sensing. *Sensors and Actuators B: Chemical,* 78(1–3), 89-97.

Eom, J.-H., Kim, Y.-W., & Raju, S. (2013). Processing and properties of macroporous silicon carbide ceramics: A review. *Journal of Asian Ceramic Societies,* 1(3), 220-242.

Haridas, D., Chowdhuri, A., Sreenivas, K., & Gupta, V. (2008). Enhanced LPG response characteristics of SnO_2 thin film based sensors loaded with Pt clusters. *Proceedings of the 3rd International Conference on Sensing Technology* (pp. 503-514). Tainan: Taiwan.

Jin, L., Chen, W., Zhou, Q., Xiao, G., & Yu, C. (2016). Detection of acetylene dissolved in transformer oil using SnO_2/rGO nanocomposite gas sensor. *Proceedings of the IEEE International Conference on Power System Technology* (pp. 1-4). Wollongong: NSW, Australia.

Kanan, S., El-Kadri, O., Abu-Yousef, I., & Kanan, M. (2009). Semiconducting Metal Oxide Based Sensors for Selective Gas Pollutant Detection. *Sensors,* 9(10), 8158.

Khadayate, R. S., Waghulde, R. B., Wankhede, M. G., Sali, J. V., & Patil, P. P. (2007). Ethanol vapour sensing properties of screen printed WO_3 thick films. *Bulletin of Materials Science,* 30(2), 129-133.

Mohanta, D., & Ahmaruzzaman, M. (2016). Tin oxide nanostructured materials: an overview of recent developments in synthesis, modifications and potential applications. *RSC Advances,* 6(112), 110996-111015.

Pimtong-Ngam, Y., Jiemsirilers, S., & Supothina, S. (2007). Preparation of tungsten oxide-tin oxide nanocomposites and their ethylene sensing characteristics. *Sensors and Actuators, A: Physical,* 139(1-2 SPEC. ISS.), 7-11.

Prasek, J., Adamek, M., Hubalek, J., Adam, V., Trnkova, L., & Kizek, R. (2006). New Hydrodynamic Electrochemical Arrangement for Cadmium Ions Detection Using Thick-Film Chemical Sensor Electrodes. *Sensors (Basel, Switzerland),* 6(11), 1498-1512.

Samson, S., & Fonstad, C. G. (1973). Defect structure and electronic donor levels in stannic oxide crystals. *Journal of Applied Physics,* 44(10), 4618-4621.

Šetkus, A., Kancleris, Z., Olekas, A., Rimdeika, R., Senuliene, D., & Strazdiene, V. (2008). Qualitative and quantitative characterization of living bacteria by dynamic response parameters of gas sensor array. *Sensors and Actuators, B: Chemical,* 130(1), 351-358.

Smilgies, D. M. (2009). Scherrer grain-size analysis adapted to grazing-incidence scattering with area detectors. *Journal of Applied Crystallography,* 42(6), 1030-1034.

Smith, D. J., Vatelino, J. F., Falconer, R. S., & Wittman, E. L. (1993). Stability, sensitivity and selectivity of tungsten trioxide films for sensing applications. *Sensors and Actuators: B. Chemical,* 13(1-3), 264-268.

Solis, J. L., Saukko, S., Kish, L., Granqvist, C. G., & Lantto, V. (2001). Semiconductor gas sensors based on nanostructured tungsten oxide. *Thin Solid Films,* 391(2), 255-260.

Suchorska-Woźniak, P., Rac, O., Fiedot, M., & Teterycz, H. (2014). Analysis of SnO_2/WO_3 heterocontact properties during the detection of hydrogen sulphide. *Sensors (Switzerland),* 14(11), 20480-20499.

Teterycz, H., & Licznerski, B. W. (2006). Properties of selective gas-sensitive $SnO_2/RuO2_2$/Pt composition and detection mechanism. *Journal of the Electrochemical Society,* 153(5), H94-H104.

Wang, C., Yin, L., Zhang, L., Xiang, D., & Gao, R. (2010). Metal oxide gas sensors: Sensitivity and influencing factors. *Sensors (Basel, Switzerland),* 10(3), 2088-2106.

Yang, J. I., Lim, H., & Han, S. D. (1999). Influence of binders on the sensing and electrical characteristics of WO_3-based gas sensors. *Sensors and Actuators, B: Chemical,* 60(1), 71-77.

Yang, J. P., Wang, W. Q., Bussolotti, F., Cheng, L. W., Li, Y. Q., Kera, S., . . . Ueno, N. (2016). Quantitative fermi level tuning in amorphous organic semiconductor by molecular doping: Toward full understanding of the doping mechanism. *Applied Physics Letters,* 109(9), 093302.

Yang, Q., & Zhao, L. R. (2008). Characterization of nano-layered multilayer coatings using modified Bragg law. *Materials Characterization,* 59(9), 1285-1291.

Authors

Dr. Yutthana Phimthong-Ngam
Physics Education Program, Faculty of Science and Technology,
Suan Dusit University
e-mail: yutthana_phi@dusit.ac.th

Trakool Rummachat
Physics Education Program, Faculty of Science and Technology,
Suan Dusit University
e-mail: trakool_rum@dusit.ac.th

Dr. Rangsan Jomtarak
Physics Education Program, Faculty of Science and Technology,
Suan Dusit University
e-mail: rangsan_jam@dusit.ac.th